Appendix A

Wavefield-based estimation of the local Snell parameter, and the propagation direction

Inversion methods that estimate the elastic parameters of the medium based on the directional dependence of the reflection coefficient (AVO inversion) use in general an angular functionality to express such a dependence. This choice is not always convenient because the angle estimation may depend strongly on the macro model that is used in the estimation process. Moreover, the propagation angles are affected by the elastic perturbations that one wishes to estimate using the angular dependence of the reflectivities. A more appropriate choice for expressing the directional dependence of the reflection coefficient is, I believe, the *local Snell parameter*, which is defined as the component of the slowness parallel to the local reflector plane at each position of the subsurface. Evidently, not all points of the subsurface can be considered as reflectors, but at all points of interest, where the upcoming wavefronts intercept the downgoing wavefront, a local reflector plane can be defined (point diffractors are an exception). As defined, the local Snell parameter is conserved for first order perturbation in the local elastic parameters. Although its estimated value still depends on the macro model, it is much less sensitive to errors in the model than the angle of incidence.

A.1 Estimation of the local Snell parameter

Figure A.1 shows a descending (incident) wavefield crossing an ascending (reflected) wavefield at a given time step of the backward propagation part of the scheme. The crossing point defines the point of the interface that was imaged at that time, and the angles α and β are measured, respectively, from the tangent and from the normal to the interface at that point. From the figure we get the following relation:

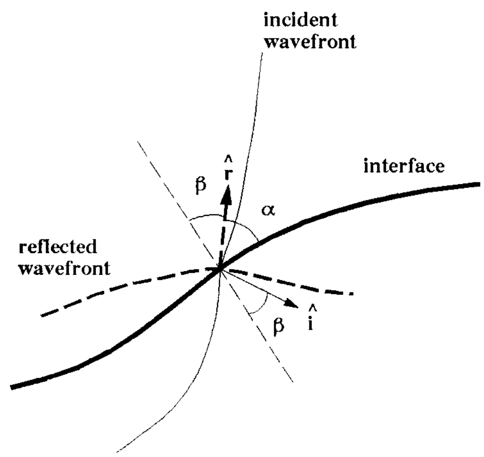

FIG. A.1. The points where the ascending and descending wavefronts overlap define the location of the reflector. The reflection angle can be determined by the gradients of the two wavefields at the reflection point at the time when the reflection occurred.

$$\cos(2\alpha) = \hat{\mathbf{i}} \cdot \hat{\mathbf{r}},$$

where the *unit vectors* $\hat{\mathbf{i}}$ and $\hat{\mathbf{r}}$ represent, respectively, the directions of incidence and reflection. I define the *local Snell parameter* $\tilde{p}$ as the slowness component parallel to the interface at the reflection point, as follows:

$$\tilde{p} \;=\; \frac{\sin(\beta)}{v_p} \;=\; \sqrt{\frac{\hat{\mathbf{i}} \cdot \hat{\mathbf{r}} + 1}{2v_p^2}}, \qquad \text{(A.1)}$$

where v_p is the P-wave group velocity at that particular location. This definition is restricted to cases in which an isotropic assumption is used, but a more general definition can be formulated that includes the anisotropic extension of Snell's law.

A.2 Estimation of the propagation direction

The unit vectors $\hat{\mathbf{i}}$ and $\hat{\mathbf{r}}$ are estimated from the potential fields ϕ^s and ϕ^r using the following equations:

$$\begin{aligned}\hat{\mathbf{i}} &= -\,\mathrm{signum}(\frac{\partial \phi^s}{\partial t})\frac{\nabla \phi^s}{\mid \nabla \phi^s \mid},\\ \hat{\mathbf{r}} &= -\,\mathrm{signum}(\frac{\partial \phi^r}{\partial t})\frac{\nabla \phi^r}{\mid \nabla \phi^r \mid}.\end{aligned} \tag{A.2}$$

The next paragraph demonstrates that these relations give the correct estimation of the propagation direction for the incident wavefield. Figure A.2 shows the wavefield amplitude along the line defined by the gradient of the potential field.

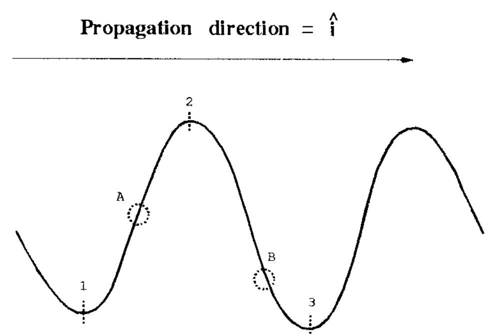

FIG. A.2. Representation of the amplitude of the potential field along the gradient direction.

The gradient of the potential field gives the direction, but not the sense of propagation. Any point A in the interval between points 1 and 2 in the figure will have a positive gradient, and any point B in the interval between points 2 and 3 will have a negative gradient. Since the propagation direction is positive (to the right), point A will have a negative time derivative, while point B will have a positive time derivative. If the propagation direction were negative (to the left), then the gradients would remain unchanged, while the time derivatives would switch signs. As a result, the product of the gradient and the time derivative at any point will have the opposite sign of the propagation direction.

Appendix B

Correlation intervals for the plane-wave decomposition imaging criterion

Figure B.1 shows a snapshot of a wavefield at the particular time and location at which a wavefront is being transmitted/converted and reflected at an interface. No conversion is observed because only the potential field of the P wave is displayed. To implement the plane-wave decomposition imaging criterion requires the computation of the slant-stacks around all points in the grid for the upcoming and the downgoing wavefields, at regular angle intervals. These stacks correspond to a semi-plane-wave decomposition around each point because they are computed from (not across) the grid points.

Let's consider the two functions $\Phi^u(\theta)$ and $\Phi^d(\theta)$, corresponding, respectively, to the stacks of the upcoming and downgoing wavefields around the intersection point of the three wavefronts (incident, transmitted, and reflected) in Figure B.1. While $\Phi^u(\theta)$ only has one maximum, in the direction tangent to the reflected wavefront at that point, $\Phi^d(\theta)$ has two local maxima; one in the direction tangent to the incident wavefront and one in the direction tangent to the transmitted wavefront. A crucial step in implementing this imaging criterion is the selection of the proper subdomain Θ^i of the distribution $\Phi^d(\theta)$, where the maximum associated with the incident wave is located.

First it is necessary to find the angle $\theta^u_{\max}$ for which $\Phi^u(\theta)$ is maximum, as follows:

$$\Phi^u(\theta^u_{\max}) = \max\left[\Phi^u(\theta)\right].$$

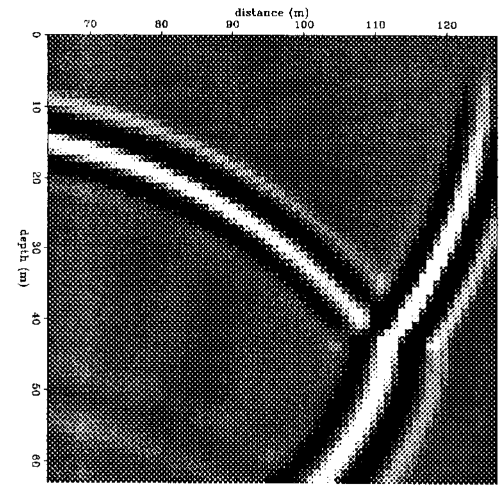

FIG. B.1. Snapshot of a wavefield propagating through an interface. The incident and transmitted wavefronts propagate downward, while the reflected wavefront propagates upward. All three wavefronts meet at the point of the interface where the partition takes place at that particular time.

As explained below, the location of the subdomain Θ^i depends on the quadrant where $\theta^u_{\max}$ is located.

The following rules are applied in the analysis:

1. The reflected wavefront can only propagate upward, and the incident wavefront can only propagate downward.

2. The reflected and incident wavefronts meet the interface at the same angle (the Snell law).

3. The reflecting interface is locally planar.

4. The incident wavefront can only propagate toward the interface, and the reflected wavefront can only propagate outward from the interface.

Figure B.2 includes four diagrams, each one corresponding to a different quadrant location for $\theta^u_{\max}$. The dark bars in each diagram refer to the limit directions of the reflected wavefront (i.e., $\theta^u_{\max}$) in each quadrant, and the arrows indicate the only possible propagation direction for this wavefront.

These are the four possibilities:

- **a) Reflected wavefront in the first quadrant**

  If the reflected wavefront is horizontal, then the incident wavefront must be restricted to the second quadrant; otherwise one of the above-stated rules would be violated.

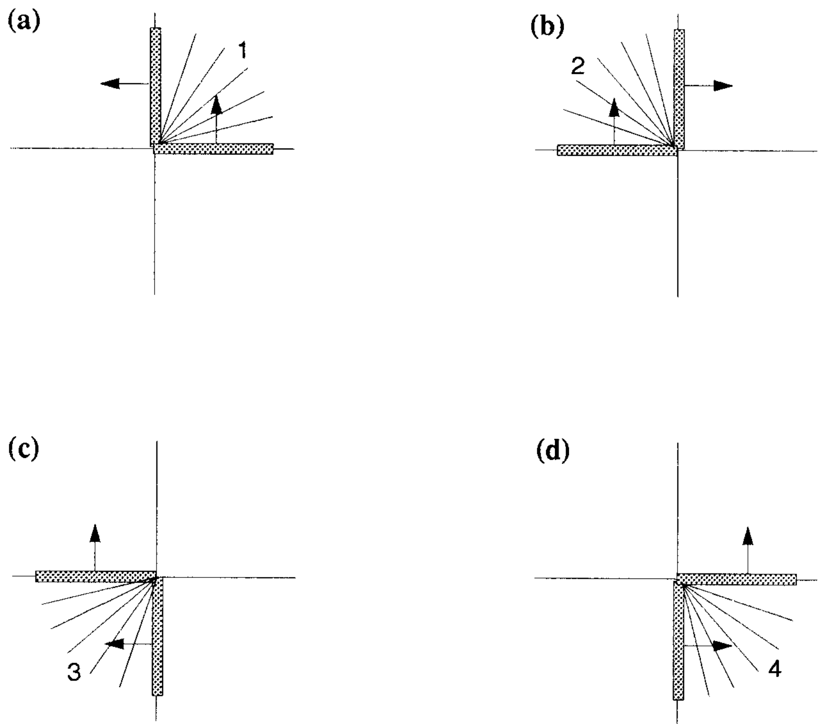

FIG. B.2. Diagrams representing the location of the reflected wavefront (dark bars) and its propagation direction (arrows). (a) The reflected wavefront is located in the first quadrant (0–$\pi/2$). (b) The reflected wavefront is located in the second quadrant ($\pi/2$–π). (c) The reflected wavefront is located in the third quadrant (π–$3\pi/2$). (d) The reflected wavefront is located in the fourth quadrant ($3\pi/2$–2π).

If the reflected wavefront is vertical, then the incident wavefront must be restricted to the second or third quadrant.

$$0 \leq \theta^u_{\max} \leq \frac{\pi}{2} \quad \longrightarrow \quad \frac{\pi}{2} \leq \theta^d \leq \frac{3\pi}{2}$$

- **b) Reflected wavefront in the second quadrant**

  If the reflected wavefront is horizontal, then the incident wavefront must be restricted to the first quadrant. If the reflected wavefront is vertical, then the incident wavefront must be restricted to the first or fourth quadrant.

$$\frac{\pi}{2} \leq \theta^u_{\max} \leq \pi \quad \longrightarrow \quad -\frac{\pi}{2} \leq \theta^d \leq \frac{\pi}{2}$$

- **c) Reflected wavefront in the third quadrant**

  If the reflected wavefront is horizontal, then the incident wavefront must be restricted to the first quadrant. If the reflected wavefront is vertical, then the incident wavefront must be restricted to the first or fourth quadrant.

$$\pi \leq \theta^u_{\max} \leq \frac{3\pi}{2} \quad \longrightarrow \quad -\frac{\pi}{2} \leq \theta^d \leq \frac{\pi}{2}$$

- **d) Reflected wavefront in the fourth quadrant**

  If the reflected wavefront is horizontal then the incident wavefront must be restricted to the second quadrant. If the reflected wavefront is vertical then the incident wavefront must be restricted to the second or third quadrants.

$$-\frac{\pi}{2} \leq \theta^u_{\max} \leq 0 \quad \longrightarrow \quad \frac{\pi}{2} \leq \theta^d \leq \frac{3\pi}{2}$$

The above relations can be summarized as

$$-\frac{\pi}{2} \leq \theta^u_{\max} \leq \frac{\pi}{2} \quad \longrightarrow \quad \frac{\pi}{2} \leq \theta^d \leq \frac{3\pi}{2}$$

$$\frac{\pi}{2} \leq \theta^u_{\max} \leq \frac{3\pi}{2} \quad \longrightarrow \quad -\frac{\pi}{2} \leq \theta^d \leq \frac{\pi}{2}.$$

Figure B.3 is a graphical representation of these relations. When the reflected wavefront is located in the first or fourth quadrant (dark bar in B.3a), the incident wavefront must be in the second or third quadrants (white bar). When the reflected wavefront is located in the second or third quadrant (dark bar in B.3b), the incident wavefront must be

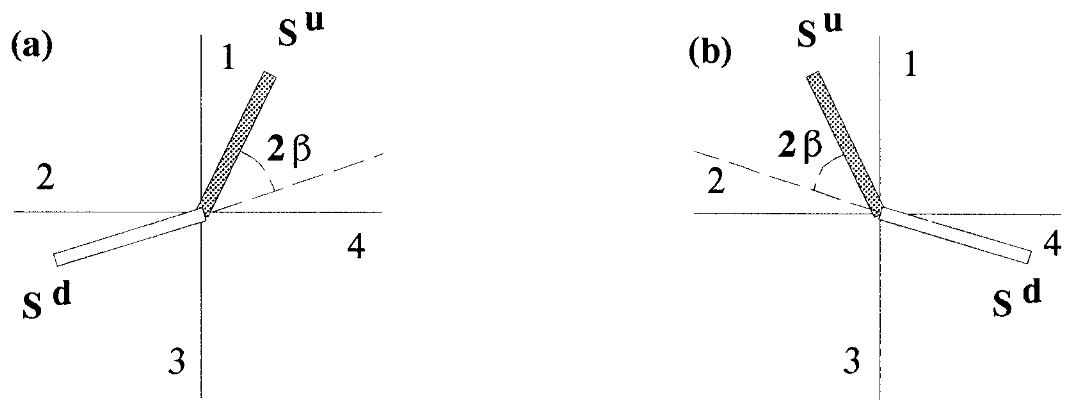

FIG. B.3. Diagrams showing the relation between the reflected (dark bar) and transmitted (white bar) wavefronts. (a) If the reflected wavefront is located in the first or fourth quadrant, the transmitted wavefront must be located in the second or third quadrant. (b) If the reflected wavefront is located in the second or third quadrant, the transmitted wavefront must be located in the first or fourth quadrant. β is the angle of incidence.

in the first or fourth quadrant (white bar). As indicated in the figure, the angle between the direction of the two wavefronts is equal to twice the angle of incidence.

Using the above relations, the correlation between the two distributions, $\Phi^u(\theta)$ and $\Phi^d(\theta)$, is given by

$$\mathcal{C}(\beta) = \sum_{\theta=\pi/2}^{3\pi/2} \left[\Phi^u(\theta - \pi + 2\beta)\, \Phi^d(\theta)\right] \qquad \text{if} \quad \frac{-\pi}{2} \le \theta^u_{\text{max}} \le \frac{\pi}{2},$$

and

$$\mathcal{C}(\beta) = \sum_{\theta=-\pi/2}^{\pi/2} \left[\Phi^u(\theta + \pi - 2\beta)\, \Phi^d(\theta)\right] \qquad \text{if} \quad \frac{\pi}{2} \le \theta^u_{\text{max}} \le \frac{3\pi}{2},$$

and the autocorrelation of $\Phi^d(\theta)$ by

$$\mathcal{A}(\beta) = \sum_{\theta=\pi/2}^{3\pi/2} \left[\Phi^d(\theta)\, \Phi^d(\theta)\right] \qquad \text{if} \quad \frac{-\pi}{2} \le \theta^u_{\text{max}} \le \frac{\pi}{2},$$

and

$$\mathcal{A}(\beta) = \sum_{\theta=-\pi/2}^{\pi/2} \left[\Phi^d(\theta)\, \Phi^d(\theta)\right] \qquad \text{if} \quad \frac{\pi}{2} \le \theta^u_{\text{max}} \le \frac{3\pi}{2}.$$

The reflectivity estimation for that particular time would be given by the ratio $\mathcal{C}/\mathcal{A}$.

Bibliography

Alford, R. M., Kelly, K. R., Boore, D. M., 1974, Accuracy of finite-difference modeling of the acoustic wave equation: Geophysics, **39**, 834–842.

Alterman, Z., and Karal, F. C., Jr., 1968, Propagation of elastic waves in layered media by finite-difference methods: Bull. Seis. Soc. Am., **58**, 367–398.

Aki, K., and Richards, P.G., 1980, Quantitative Seismology, vol. I: First edition, Freeman and Company, 273–286.

Auld, B.A. , 1990, Acoustic fields and waves in solids, vol. I: Second edition, Krieger Publishing Company, 142–145.

Backus, G.E., 1962, Long-wave elastic anisotropy produced by horizontal layering: J. Geophys. Res., **67**, 4427–4440.

Backus, G.E. and Gilbert, J.F., 1967, Numerical application of a formalism for geophysical inverse problems: Geophys. J. Roy. Astron. Soc., **13**, 247–276.

Backus, G.E. and Gilbert, J.F., 1968, The resolving power of gross earth data: Geophys. J. Roy. Astron. Soc., **16**, 169–205.

Backus, G.E. and Gilbert, J.F., 1970, Uniqueness in the inversion of gross earth data: Phil. Trans. Roy. Soc. London, Ser. A., **266**, 123–192.

Baysal, E., Kosloff, D.D., and Sherwood, J.W.C., 1983, Reverse time migration: Geophysics, **48**, 1514–1524.

Boore, D. M., 1970, Finite-difference solutions to the equations of elastic wave propagation, with application to Love waves over dipping interfaces: Ph.D. thesis, M.I.T

Bruin, C.G.M., Wapenaar, C.P.A., and Berkhout, A.J., 1988, Angle-dependent reflectivity by shot record migration: 58th Annual Internat. Mtg., Soc. Expl. Geophys., Expanded Abstracts, 1093–1096.

Bruin, C.G.M. de, Wapenaar, C.P.A., and Berkhout, A.J., 1990a Angle-dependent reflectivity by means of prestack migration: Geophysics, **55**, 1223–1234.

Bruin, C.G.M. de, Wapenaar, C.P.A., and Berkhout, A.J., 1990b Imaging for angle-dependent reflectivity in the presence of dip: 60th Ann. Internat. Mtg., Soc. Expl. Geophys., Expanded Abstracts, 1503–1506.

Bruin C. G. de, and Wapenaar, C. P. A., 1991, Target-Oriented Tau-P Gathers for AVO Inversion: 61st Annual Internat. Mtg., Soc. Expl. Geophys., Expanded Abstracts, 1095–1097.

Cerjan, C., Kosloff, D., Kosloff, R., and Reshef, M., 1985, A nonreflecting boundary condition for discrete acoustic and elastic wave equations: Geophysics, **50**, 705–708.

Chang, W.F., and McMechan, G.A., 1987, Elastic reverse-time migration: Geophysics, **52**, 1365–1375.

Cheng, C.H., and Toksöz, M.N., 1979, Inversion of seismic velocities for the pore aspect ratio spectrum of a rock: J. Geophys. Res., **84**, 7533–7543.

Claerbout, J.F., 1971, Toward a unified theory of reflector mapping: Geophysics, **36**, 467–481.

Claerbout, J.F., 1985, Imaging the Earth's Interior: Blackwell Scientific Publications.

Claerbout, J.F., 1992a, Earth Soundings Analysis: Processing versus Inversion: Blackwell Scientific Publications.

Claerbout, J.F., 1992b, Spatial aliasing: SEP-**73**, 367–369.

Clayton, R.W., 1981, Wavefield inversion methods: a proposal: PhD thesis, Stanford University, also SEP-**27**.

Cohen, J.K., and Bleistein N., 1977, An inverse method for determining small variations in propagation speed: SIAM J. Apl. Math., **32**, 784–799.

Cohen, J.K., and Bleistein N., 1979, Velocity inversion procedure for acoustic waves: Geophysics, **44**, 1077–1087.

Cunha Filho, C.A., 1990, Snell-beam transform: Retrieving the angle-dependent reflectivity: 60th Annual Internat. Mtg., Soc. Expl. Geophys., Expanded Abstracts, 1507–1510.

Cunha Filho, C.A., 1991a, Model decomposition with Walsh functions in non-linear traveltime inversion: SEP-**70**, 193–200.

Cunha Filho, C.A., 1991b, Modeling a discrete system by eigenvalue decomposition: SEP–**72**, 55–71.

Dablain, M.A., 1986, The application of high-order differencing to the scalar wave equation: Geophysics, **51**, 54–66.

Demirbag, E., and Coruh, C., 1989, Inversion of Multilayer Amplitude versus Offset Data: 59th Annual Internat. Mtg., Soc. Expl. Geophys., Expanded Abstracts, 709–712.

Domenico, S.N., 1976, Effect of Brine-Gas Mixture on velocity in an unconsolidated sand reservoir: Geophysics, **41**, 882–894.

Domenico, S.N., 1984, Rock lithology and porosity determination from shear and compressional wave velocity: Geophysics, **49**, 1188-1195.

Etgen, J.T, 1986, Prestack reverse-time migration of shot profiles: SEP–**50**, 151–169.

Etgen, J.T, 1987, Finite-difference elastic anisotropic wave propagation: SEP–**56**, 23–57.

Etgen, J.T., 1989, Accurate wave equation modeling: SEP–**60**, 131–147.

Faria, E.L, Lowental, D., Stoffa, P.L., 1986, Migration before stack using reverse time propagation: 56th Ann. Internat. Mtg., Soc. Expl. Geophys., Expanded Abstracts, 257–260.

de Haas, J.C., and Berkhout, A.J., 1988, On the information content of P-P, P-SV, SV-SV, and SV-P reflections: 58th Annual Internat. Mtg., Soc. Expl. Geophys., Expanded Abstracts, 1190–1193.

Hale, D.T., 1990, 3-D depth migration via McClellan transformations: 60th Annual Internat. Mtg., Soc. Expl. Geophys., Expanded Abstracts, 1325–1328.

Han, D.H., Nur, A., and Morgan D., 1986, Effects of porosity and clay content on wave velocities in sandstones: Geophysics, **51**, 2093–2107.

Hellman, K.J, 1986, Evaluation of a reverse-time prestack migration algorithm: 56th Annual Internat. Mtg., Soc. Expl. Geophys., Expanded Abstracts, 330–332.

Hildebrand, S.A., 1987, Reverse-time depth migration: Impedance imaging condition: Geophysics, **52**, 1060–1064.

Hindlet, P., and Kolb, P., 1988, Inversion of pre-stack field data: An application to 1D acoustic media: 58th Annual Internat. Mtg., Soc. Expl. Geophys., Expanded Abstracts, 1073–1076.

Hornby B.E., and Murphy, W.F., 1987, V_p/V_s in unconsolidated oil sands: Shear from Stoneley: Geophysics, **52**, 502–513.

Jacobs, A., 1982, The pre-stack migration of profiles: Ph.D. thesis, Stanford University.

Jannane M., Beydoun, W., Crase, E., Cao, D. Koren, Z, Landa, E., Mendes, M., Pica, A., Noble, M., Roeth, G., Singh, S., Snieder, R., Tarantola, A., Trezeguet, D., and Zie, M., 1989, Wavelengths of earth structures that can be resolved from seismic reflections data: Geophysics, **54**, 906–910.

Karrenbach, M., 1991, Prestack reverse-time migration in anisotropic media: SEP–**70**, 113–121.

Keith, C.M., and Crampin, S., 1977, Seismic body waves in anisotropic media: reflection and refraction at a plane interface: Geophys. J. R. Soc., **49**, 181–208.

Kelly, K. R., Ward, R. W., Treitel, S., and Alford, R. M., 1976, Synthetic seismograms: A finite-difference approach: Geophysics, **41**, 2–27.

Kolb, P., Chapel, F., and Picart, R., 1989, Lithologic inversion: A reflectivity versus angle (RVA) approach: 60th Annual Internat. Mtg., Soc. Expl. Geophys., Expanded Abstracts, 695–699.

Kosloff, D.D., and Baysal, E., 1983, Migration with the full acoustic wave equation: Geophysics, **48**, 677–687.

Kosloff, D., Reshef, M., and Lowenthal, D., 1984, Elastic waves calculations by the Fourier method: Bull. Seis. Soc. Am., **74**, 875–891.

Lanning, E.N., and Johnson, D.M., 1983, Automated identification of rock boudaries: An application of the Walsh transform to geophysical well-log analysis: Geophysics, **48**, 197–205.

Levin, S., 1984, Principle of reverse-time migration: Geophysics, **49**, 581–583.

Lowenthal, D., and Mufti, I.R., 1983, Reverse time migration in spatial frequency domain: Geophysics, **48**, 627–635.

Lumley, D.E., and Beydoun, W.B., 1991, Elastic parameter estimation by Kirchhoff prestack depth migration/inversion: SEP–**70**, 165–192.

Marfurt, K.J., 1984, Accuracy of finite-difference and finite-element modeling of the scalar and elastic wave equations: Geophysics, **49**, 533–549.

McMechan, G. A., 1983, Migration by extrapolation of time-dependent boundary values: Geophys. Prosp., **31**, 413–420.

Monk, D.J., 1990, Wavefield separation of twin streamer data: First Break, **8**, 96-104.

Mora, P., 1986, Elastic finite-differences with convolutional operators: SEP–**48**, 151–169.

Mora, P., 1987a, Nonlinear two-dimensional elastic inversion of multioffset seismic data: Geophysics, **52**, 1211–1228.

Mora, P., 1987b, Elastic wavefield inversion: PhD Thesis, Stanford University, also SEP-**52**.

Newman, P., 1973, Divergence effects in a layered earth: Geophysics, **38**, 481–488.

O'Doherty, R.F., and Anstey N.A., 1971, Reflection on amplitudes: Geophys. Prosp., **19**, 430–458.

Ostrander, W.J., 1984, Plane-wave reflection coefficients for gas sands at non normal angles of incidence: Geophysics, **49**, 1637–1648.

Ottaviani, Mario, 1971, Elastic wave propagation in two evenly welded quarter-spaces: Bull. Seis. Soc. Am., **61**, 1119–1152.

Rosa, A.L., and Schinelli, M.C., 1985, Deconvolution tests with deep water experimental data from Campos basin, Brazil: 55th Annual Internat. Mtg., Soc. Expl. Geophys., Expanded Abstracts, 491–495.

Schlumberger log interpretation principles, 1989: Schlumberger educational services.

Sheriff, R.E., 1975, Factors affecting seismic amplitudes: Geophys. Prosp., **23**, 125–138.

Shoenberg, M., and Muir, F., 1989, A calculus for finely layered anisotropic media: Geophysics, **54**, 581–589.

Shoenberg, M., and Protazio, J., 1990, Zoeppritz rationalized and generalized to anisotropy: Presented at the ASA SanDiego Mtg.

Snieder, R., Xie, M.Y., Tarantola, A., and Pica, A., 1988, Retrieving Both the impedance Variations and Background Velocity in Reflection Seismics Using Least-Squares Waveform Inversion: 58th Annual Internat. Mtg., Soc. Expl. Geophys., Expanded Abstracts, 1070–1072.

Tarantola, A., 1984, Inversion of seismic reflection data in the acoustic approximation: Geophysics, **49**, 1259–1266.

Tarantola, A., 1986, A strategy for nonlinear elastic inversion of seismic reflection data: Geophysics, **51**, 1893–1903.

Uren, N.F., Gardner, G.H.F., and McDonald, J.A., 1990, The migrator's equation for anisotropic media: Geophysics, **55**, 1429–1434.

Virieux, J., 1984, SH wave propagation in heterogeneous media: Velocity-stress finite-difference method: Geophysics, **49**, 1933–1937.

Virieux, J., 1986, P-SV wave propagation in heterogeneous media: Velocity-stress finite-difference method: Geophysics, **51**, 889–901.

Wapenaar, C. P. A., Verschuur, D. J., and Herrmann, P., 1990, Amplitude Preprocessing of 2-D Seismic Data: 60th Annual Internat. Mtg., Soc. Expl. Geophys., Expanded Abstracts, 1491–1494.

Whitmore, N.D., 1984, Interactive Depth Migration by Backward time propagation: 53th Annual Internat. Mtg., Soc. Expl. Geophys., Expanded Abstracts, – .

Wyllie, M.R.J., Gregory, A.R., and Gardner, G.H.F., 1956, Elastic waves velocities in heterogeneous and porous media: Geophysics, **21**, – .

Yu, G., 1985, Offset-amplitude variation and controlled-amplitude processing: Geophysics, **50**, 2697–2708.